Structural Defects

International Edition: DOI: 10.1002/anie.201907074
German Edition: DOI: 10.1002/ange.201907074

Switching on the Photocatalysis of Metal–Organic Frameworks by Engineering Structural Defects

Xing Ma[+], Li Wang[+], Qun Zhang, and Hai-Long Jiang**

Abstract: *Defect engineering is a versatile approach to modulate band and electronic structures as well as materials performance. Herein, metal–organic frameworks (MOFs) featuring controlled structural defects, namely UiO-66-NH_2-X (X represents the molar equivalents of the modulator, acetic acid, with respect to the linker in synthesis), were synthesized to systematically investigate the effect of structural defects on photocatalytic properties. Remarkably, structural defects in MOFs are able to switch on the photocatalysis. The photocatalytic H_2 production rate presents a volcano-type trend with increasing structural defects, where Pt@UiO-66-NH_2-100 exhibits the highest activity. Ultrafast transient absorption spectroscopy unveils that UiO-66-NH_2-100 with moderate structural defects possesses the fastest relaxation kinetics and the highest charge separation efficiency, while excessive defects retard the relaxation and reduce charge separation efficiency.*

Defects, disruptions of the periodic atomic arrangements in the crystal lattice, are almost universal in the structure of solid materials, despite the great efforts made to achieve minimum-energy systems.[1] The formation of structural defects is generally accompanied by bond breaking and reforming, lattice distortion, and electron localization, which induce property changes in various applications. For instance, short-range disordered structural defects can behave as scattering centers by breaking electronic structure and causing localized band-tail states, thus affecting the mobility and conductivity.[1] Therefore, defects have long been regarded as unfavorable imperfections that can deteriorate the performance of materials.[2] In contrast, in-depth experimental and theoretical studies recently revealed the importance of defects in tailoring the local properties of solid materials and endowing them with new functionalities and/or enhanced performances.[3] Particularly, the control of lattice defects in semiconductive materials may be able to modulate the electronic and band structures, carrier concentration, and even the conductivity.[3] Moreover, from the perspective of surface science and catalysis, the coordinatively unsaturated sites associated with surface defects can serve as active sites for molecular absorption and activation.[4] Therefore, the rational creation of structural defects may offer the opportunity to tune and optimize the performance. Given the subtle influence of defects on properties, especially catalysis, it is of great importance to employ a suitable model and rationally engineer structural defects for a deeper understanding of the relationship between defect control and performance.

Metal–organic frameworks (MOFs), a class of crystalline porous material, are assembled from inorganic metal ions/clusters and organic linkers.[5] The periodic and well-defined structures of MOFs make them ideal candidates for defect studies. Starting from perfect single-crystal structures, the rational introduction of structural defects into MOFs is feasible by regulating the synthetic parameters that may affect the properties. Owing to the unique advantages of MOFs, including high surface area, well-exposed active sites, and free transport of substrates/products in the pores, there have been intensive explorations toward catalysis and photocatalysis based on their structural modulation and decoration in recent years.[6] Although a few recent investigations on MOF defects have suggested preliminary influences on catalysis and sorption,[7] to the best of our knowledge, there has never been experimental exploration to clarify how different levels of structural defects in MOFs systematically affect the photocatalytic performance.

As a representative MOF, UiO-66-NH_2[8] was chosen for this study due to its facile synthesis, great stability, structural tailorability, and high tolerance for structural modulation.[7] Previous theoretical studies have indicated that the removal of linkers in UiO-66 lowers energy levels of the unoccupied d orbitals of Zr atoms, which may increase the likelihood of charge transfer in the photocatalytic process.[9] In this context, with controlled defect engineering, UiO-66-NH_2 may be an ideal platform to systematically investigate the relationship between structural defects (level) and photocatalytic performance.

Bearing these considerations in mind, we have rationally synthesized UiO-66-NH_2 with different contents of structural defects, denoted as UiO-66-NH_2-X (where X = 0, 50, 100, 150, 200, representing the molar equivalents of the modulator with respect to the linker upon synthesis), for photocatalytic H_2

[*] X. Ma,[+] Prof. Dr. H.-L. Jiang
Hefei National Laboratory for Physical Sciences at the Microscale
CAS Key Laboratory of Soft Matter Chemistry, Collaborative Innovation Center of Suzhou Nano Science and Technology
Department of Chemistry
University of Science and Technology of China
Hefei, Anhui 230026 (P. R. China)
E-mail: jianglab@ustc.edu.cn
Homepage: http://staff.ustc.edu.cn/~jianglab/
L. Wang,[+] Prof. Dr. Q. Zhang
Hefei National Laboratory for Physical Sciences at the Microscale
Synergetic Innovation Center of Quantum Information and Quantum Physics, Department of Chemical Physics
University of Science and Technology of China
Hefei, Anhui 230026 (P. R. China)
E-mail: qunzh@ustc.edu.cn
[+] These authors contributed equally to this work.
Supporting information and the ORCID identification number(s) for the author(s) of this article can be found under: https://doi.org/10.1002/anie.201907074.

production, in the presence of Pt nanoparticles (NPs) as co-catalyst (Scheme 1). Along with the increase in structural defects, the photocatalytic H_2 production rate gradually increases. However, unlike previous reports,[6f,9a] the photocatalytic activity gradually decreases with further increases in defect contents (X = 150, 200). Therefore, the activity of Pt@UiO-66-NH_2-X presents an evident volcano-type trend, with the highest point at X = 100. Resorting to femtosecond time-resolved transient absorption spectroscopy, the relationship between charge separation efficiency and defect levels of UiO-66-NH_2-X has been studied to understand this volcano-type trend in the photocatalytic behavior. As far as we know, this is the first experimental demonstration on the different roles of MOF defects in photocatalysis, highlighting the importance of moderate structural defects.

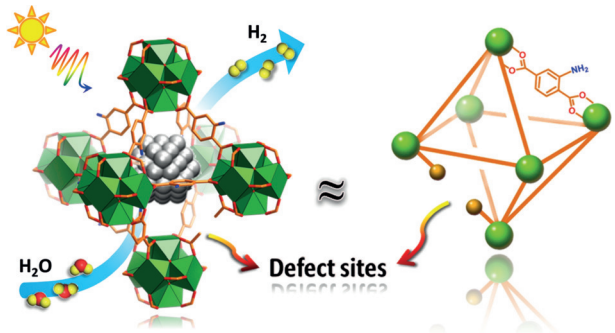

Scheme 1. Photocatalytic hydrogen production over Pt@UiO-66-NH_2-X with structural defects.

UiO-66-NH_2-X with different structural defect contents were prepared by the reaction of $ZrCl_4$ and 2-amino-1,4-benzenedicarboxylic acid (NH_2-BDC) in *N,N*-dimethylformamide, with trace amounts of water and different equivalents of acetic acid (HOAc) as modulator; the working principle of the modulator in defect formation was illustrated in detail (see the Supporting Information, Section 6). All UiO-66-NH_2-X MOFs (X = 0, 50, 100, 150, 200) show similar powder X-ray diffraction (XRD) patterns, suggesting their good crystallinity (Figure 1 a). Scanning electron microscopy (SEM) observation indicates that the MOF particles gradually change from small and intergrown prototypes to individual and octahedral nanocrystals, along with increasing particle sizes until X = 100 (Figure S1).

Several techniques have been adopted to investigate the degree of structural defects in UiO-66-NH_2-X. First, thermogravimetric analysis (TGA) curves of five UiO-66-NH_2-X are qualitatively similar and present two well-resolved weight loss steps (Figure 1 b). The weight loss in the range of 25–320 °C mainly corresponds to the loss of H_2O adsorbate and HOAc modulator. As the temperature increases up to 500 °C, the NH_2-BDC linker fully combusts with complete collapse of the framework, as verified by the intense exothermic peak in the differential thermal analysis (DTA) curves. The final residue can be mainly assigned to the monoclinic ZrO_2 with some cubic ZrO_2 (Figure S2); this is normalized to 100 % for all samples to facilitate comparison (Figure 1 b). Notably, the last weight loss step can be applied to compare the defect degree in different samples.[7c,d] The magnitude of weight loss in the last step corresponding to linker/framework combustion gradually decreases from UiO-66-NH_2-0 to UiO-66-NH_2-200 (Figure 1 b), indicating that the linker content in MOFs gradually decreases and more defects exist, exactly as expected. Therefore, it can be established that the amount of modulator in the synthetic process is inversely correlated to the amount of weight loss, while it is positively correlated to the defect degree in UiO-66-NH_2-X.

We then resorted to the dissolution/^{1}H NMR analysis, an effective tool to identify the ratio of the NH_2-BDC linker and the HOAc modulator coordinated to the Zr-oxo clusters (Figure 1 c).[7d] A significant signal enhancement assignable to CH_3COO^- can be observed in the ^{1}H NMR spectra of digested UiO-66-NH_2-X with gradually increasing X values, suggesting the incremental replacement of the linker by the HOAc modulator. Intuitively, when the dicarboxylate linker is replaced by an end-capped monocarboxylate modulator, additional pore space would be created in the MOF, which leads to higher surface area and affects the properties of UiO-66-NH_2-X.[7a] Not surprisingly, N_2 uptake gradually increases for UiO-66-NH_2-X synthesized with a higher ratio of HOAc modulator (Figure 1 d). Consequently, the Brunauer–Emmett–Teller (BET) surface area of the MOFs increases from 705 to 1057 $m^2 g^{-1}$ and the pore volume increases from 0.53 to 0.62 $cm^3 g^{-1}$, for UiO-66-NH_2-X with increased X and more defects (Table S1), while the pore size distribution does not change significantly (Figure S3). Notably, the influence of structural defects on the stability of UiO-66-NH_2 has been

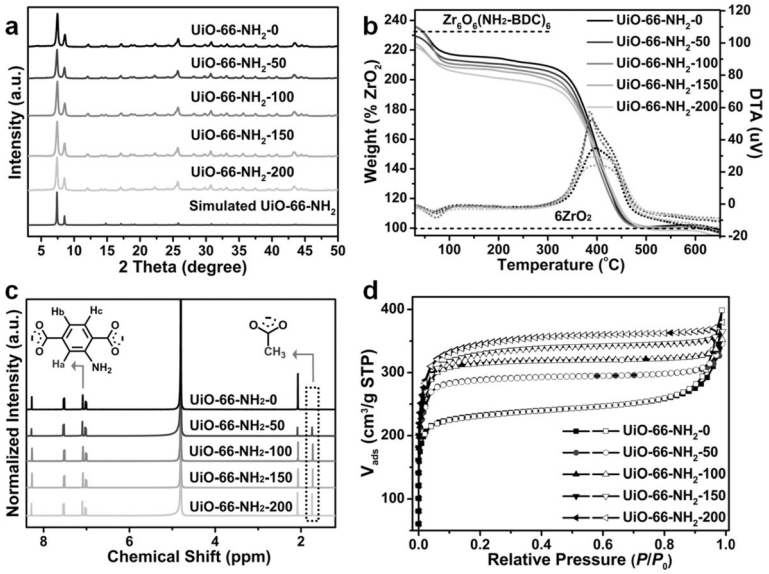

Figure 1. a) Powder XRD patterns, b) TGA plots (solid, the end weight of ZrO_2 is normalized to 100 %) and DTA (dashed) curves, c) dissolution/^{1}H NMR spectra (the intensity of H_a atom on the benzene ring is normalized to 100 a.u.), and d) nitrogen adsorption/desorption (solid/open symbols) isotherms at 77 K for UiO-66-NH_2-X (X = 0, 50, 100, 150, 200).

demonstrated to be negligible (Figures S4–S6). Moreover, the type of structural defects in UiO-66-NH_2-X is believed to be the missing linkers, according to our reaction conditions and previous reports.[7e,j,k,9b]

The UV/Vis spectra of all UiO-66-NH_2-X MOFs show similar curves in the range 250–800 nm (Figures S7–S11), and the calculated band gap for all MOFs is ≈3.0 eV (Table S2). The results indicate that the light-harvesting ability of these UiO-66-NH_2-X MOFs with a slight change in color (Figure S12) is hardly influenced by structural defects or particle size.[9a]

To boost the transfer and utilization of charge carriers in UiO-66-NH_2-X for photocatalysis, ≈1 wt% Pt NPs as co-catalyst was incorporated into the MOFs to afford Pt@UiO-66-NH_2-X composites (Table S3). This was done by adding UiO-66-NH_2-X to the Pt precursor solution, followed by reduction at 200 °C in an H_2/Ar atmosphere.[10] Powder XRD patterns suggest that the introduction of Pt NPs does not affect the crystallinity of UiO-66-NH_2-X (Figure S13). Transmission electron microscopy (TEM) observation indicates that Pt NPs with an average size of 1.2–1.4 nm are dispersed evenly in UiO-66-NH_2-X particles (Figure 2a,b, Figures S14–S18).

Next, we set out to investigate the photocatalytic H_2 production over Pt@UiO-66-NH_2-X with triethanolamine (TEOA) as a sacrificial agent. Pt@UiO-66-NH_2-0, in which the MOF features few structural defects, was synthesized without modulator and presents negligible H_2 production (9.4 μmol g^{-1} h^{-1}). The very poor activity of Pt@UiO-66-NH_2-0 may be attributed to the lack of overlap between the empty d orbitals of Zr^{4+} and the π* orbital of the linker and the obstruction of electron transfer from the linker to Zr^{4+}.[6f,9a] MOFs having more structural defects, Pt@UiO-66-NH_2-50 and Pt@UiO-66-NH_2-100, exhibit much enhanced H_2 production rates of 154.2 and 381.2 μmol g^{-1} h^{-1}, respectively, suggesting that structural defects play a critical role in photocatalysis. However, the photocatalytic activity of Pt@UiO-66-NH_2-150 and Pt@UiO-66-NH_2-200, with further incremental structural defects, drops to 302.1 and 276.8 μmol g^{-1} h^{-1}, respectively. Therefore, the photocatalytic activity shows a volcano-type trend on the whole, and Pt@UiO-66-NH_2-100 presents the highest activity among all the investigated photocatalysts (Figure 2c, Figure S19a). Moreover, Pt@UiO-66-NH_2-100 is well recyclable for at least 10 cycles (Figure 2d, Figure S19b), and its structure can be well retained, without any noticeable leaching or aggregation occurred to Pt NPs, after photocatalytic cycles (Figures S20 and S21). The impressive volcano-type trend explicitly shows that, though a suitable content of structural defects is favorable, too high concentration is detrimental to the activity. In addition, as a preliminary demonstration, the tandem reaction of photocatalytic H_2 production and nitrobenzene hydrogenation over Pt@UiO-66-NH_2-100 can be promoted in the absence of an additional hydrogen source (Figure S22).

To better understand the mechanism behind the observed volcano-type trend in activity, we resorted to femtosecond time-resolved transient absorption (fs-TA) spectroscopy to examine the charge separation processes involved.[11] In the fs-TA measurements with a pump–probe configuration, the pump was set at 400 nm, a wavelength suitable for promoting electrons from the highest occupied molecular orbital (HOMO) to the lowest unoccupied molecular orbital (LUMO) of UiO-66-NH_2, whereas the probe was from a white-light-continuum source covering a spectral region of 500–700 nm. Representative fs-TA spectra recorded for UiO-66-NH_2-0 and UiO-66-NH_2-100 show that different levels of structural defects bring on no essential variation in the spectral profile (Figure 3a). However, pronounced changes can be detected in their kinetic behavior (Figure 3b). Considering that relaxation kinetics usually depends on the probing wavelength, we conducted a global fit to retrieve the relaxation constants, in which a set of kinetic traces ranging from 580 to 650 nm with a 10 nm interval were used. The fitting results are as follows: $\tau_1 = 81 \pm 2$ ps (54%) and $\tau_2 = 689 \pm 24$ ps (46%) for UiO-66-NH_2-0; $\tau_1 = 67 \pm 2$ ps (55%) and $\tau_2 = 617 \pm 23$ ps (45%) for UiO-66-NH_2-50; $\tau_1 = 20 \pm 1$ ps (29%) and $\tau_2 = 384 \pm 5$ ps (71%) for UiO-66-NH_2-100; $\tau_1 = 174 \pm 5$ ps (61%) and $\tau_2 = 1062 \pm 59$ ps (39%) for UiO-66-NH_2-150; and $\tau_1 = 218 \pm 6$ ps (70%) and $\tau_2 = 1492 \pm 113$ ps (30%) for UiO-66-NH_2-200. The average relaxation lifetimes are 615 ± 22, 553 ± 21, 376 ± 5, 881 ± 53, and 1167 ± 101 ps for UiO-66-NH_2-X (X = 0, 50, 100, 150, 200, respectively), as also annotated in Figure 3b. As compared in Figure 3c, the variation of such a set of average relaxation lifetimes presents an exactly inverse relation to the observed volcano-type trend of H_2 production rates at different defect levels (X = 0–100; 100–200). The average relaxation lifetime can be employed as an indicator to evaluate charge separation efficiency: the faster

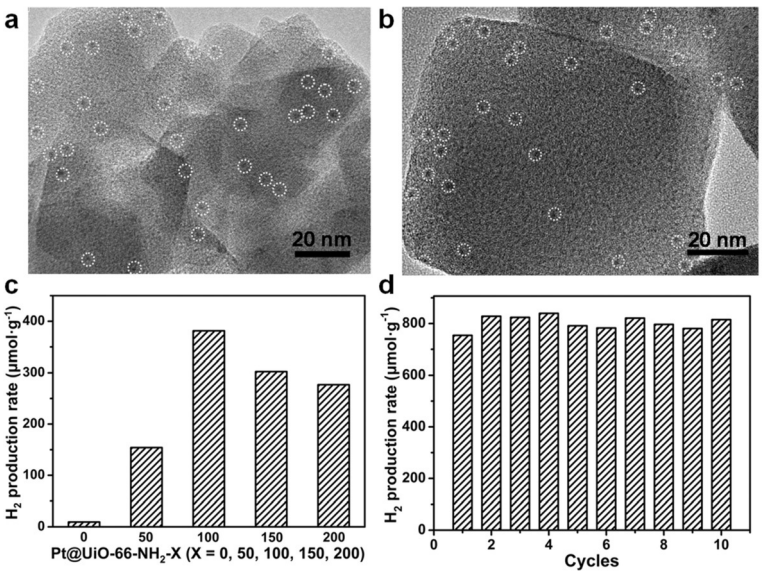

Figure 2. Typical TEM images of a) Pt@UiO-66-NH_2-0 and b) Pt@UiO-66-NH_2-100, c) photocatalytic H_2 performance from water splitting over different catalysts in MeCN/TEOA/H_2O (10.8:1:0.2 v/v, 30 mL) under light irradiation, d) recycling performance of Pt@UiO-66-NH_2-100 (2 h per cycle).

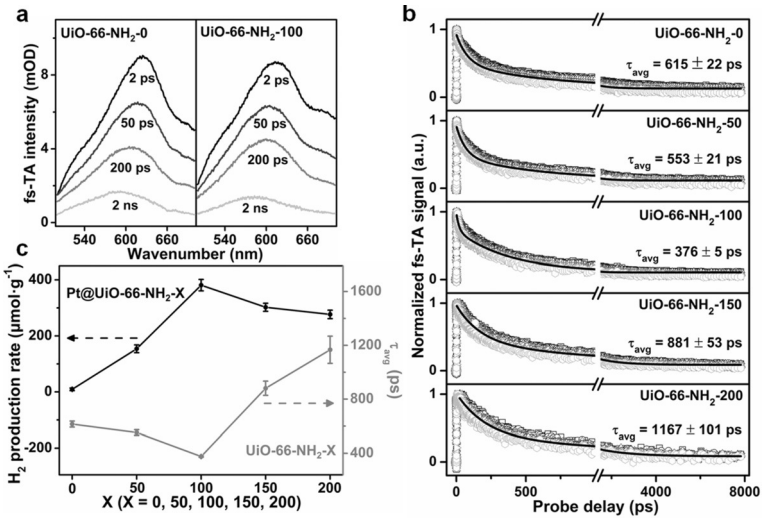

Figure 3. a) The fs-TA spectra (pump at 400 nm) taken at several representative probe delays for UiO-66-NH_2-0 and UiO-66-NH_2-100. b) fs-TA kinetics and the global fitting results (probing in the range 580–650 nm using 8 traces with a 10-nm interval) for UiO-66-NH_2-X (X = 0, 50, 100, 150, 200). c) Comparison of photocatalytic H_2 production rates and average relaxation lifetimes.

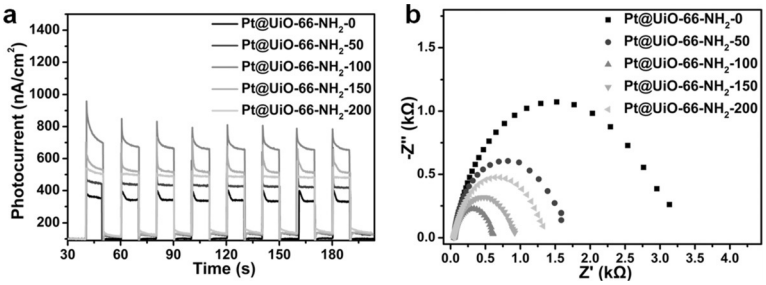

Figure 4. a) Photocurrent tests and b) EIS plots of Pt@UiO-66-NH_2-X (X = 0, 50, 100, 150, 200).

the relaxation, the higher the efficiency. The fastest relaxation observed in UiO-66-NH_2-100 is synchronous with the most predominant H_2 production rate of Pt@UiO-66-NH_2-100, indicating that UiO-66-NH_2-100 with a moderate defect level achieves the highest charge separation efficiency. It is worth noting that the average relaxation lifetimes of UiO-66-NH_2-X (X = 150, 200) are longer than those of UiO-66-NH_2-X (X = 0, 50), again indicating that the too high defect density in UiO-66-NH_2-X (X = 150, 200) is not beneficial for promoting electron–hole separation efficiency.

Transient photocurrent measurements and electrochemical impedance spectroscopy (EIS) were conducted to further verify the volcano-type trend in the activity of Pt@UiO-66-NH_2-X photocatalysts. As expected, Pt@UiO-66-NH_2-100 presents the highest photocurrent response among all the samples (Figure 4a), implying that the creation of the optimal level of structural defects is vital to the efficient separation of photogenerated electron–hole pairs, such that photocatalysis is switched on. This judgment is further supported by the EIS results (Figure 4b), where Pt@UiO-66-NH_2-100 exhibits the smallest radius, manifesting the lowest charge-transfer resistance. Combined with the above results, it is assumed that moderate defect levels may cause a decrease in energy of the unoccupied d orbitals of Zr atoms and benefit the separation and transfer of photogenerated charge,[9a] while excessive structural defects, conversely, can turn into recombination centers of electron–hole pairs, thus causing reduced activity.[3e,12]

In summary, we selected UiO-66-NH_2 as a model for the systematical investigation of the specific influence of structural defects on photocatalysis. The photocatalytic H_2 production presents an interesting volcano-type trend along with incremental levels of structural defects in the MOF. Impressively, Pt@UiO-66-NH_2-100, with an optimized content of structural defects, possesses the highest photocatalytic activity, highlighting that the creation of moderate structural defects is vital to promoting the efficient electron–hole separation. Remarkably, the significant distinction of charge separation efficiency caused by different defect levels has been systematically evidenced by fs-TA spectroscopy in terms of relaxation kinetics. Taken together, these results unambiguously demonstrate that the creation of structural defects can switch on photocatalysis and its content optimization is critical to photocatalytic performance. This work provides significant inspiration for the creation of structural defects in functional materials to optimize performance, particularly in semiconductor(-like) materials for enhanced photocatalysis.

Acknowledgements

This work was supported by the NSFC (21725101, 21673213, 21871244, 21521001, 21573211, 21633007), the MOST (2016YFA0200602, 2018YFA0208702), Fujian Institute of Innovation (Chinese Academy of Sciences), and Anhui Initiative in Quantum Information Technologies (AHY090200).

Conflict of interest

The authors declare no conflict of interest.

Keywords: defects · hydrogen production · metal–organic frameworks · photocatalysis · transient absorption

How to cite: *Angew. Chem. Int. Ed.* **2019**, *58*, 12175–12179
Angew. Chem. **2019**, *131*, 12303–12307

[1] a) G. Li, G. R. Blake, T. T. M. Palstra, *Chem. Soc. Rev.* **2017**, *46*, 1693; b) V. Lordi, P. Erhart, D. Åberg, *Phys. Rev. B* **2010**, *81*, 235204.

[2] a) F. Banhart, J. Kotakoski, A. V. Krasheninnikov, *ACS Nano* **2011**, *5*, 26; b) H. Terrones, R. Lv, M. Terrones, M. S. Dresselhaus, *Rep. Prog. Phys.* **2012**, *75*, 062501.

[3] a) X. Pan, M.-Q. Yang, X. Fu, N. Zhang, Y.-J. Xu, *Nanoscale* **2013**, *5*, 3601; b) J. Nowotny, M. A. Alim, T. Bak, M. A. Idris, M. Ionescu, K. Prince, M. Z. Sahdan, K. Sopian, M. A. M. Teridi, W. Sigmund, *Chem. Soc. Rev.* **2015**, *44*, 8424; c) D. Yan, Y. Li, J. Huo, R. Chen, L. Dai, S. Wang, *Adv. Mater.* **2017**, *29*, 1606459; d) G. Wang, Y. Yang, D. Han, Y. Li, *Nano Today* **2017**, *13*, 23; e) W. Zhou, H. Fu, *Inorg. Chem. Front.* **2018**, *5*, 1240; f) P. Yang, H. Zhuzhang, R. Wang, W. Lin, X. Wang, *Angew. Chem. Int. Ed.* **2019**, *58*, 1134; *Angew. Chem.* **2019**, *131*, 1146.

[4] a) G. Xi, S. Ouyang, P. Li, J. Ye, Q. Ma, N. Su, H. Bai, C. Wang, *Angew. Chem. Int. Ed.* **2012**, *51*, 2395; *Angew. Chem.* **2012**, *124*, 2445; b) A. Walsh, A. Zunger, *Nat. Mater.* **2017**, *16*, 964.

[5] a) H.-C. Zhou, S. Kitagawa, *Chem. Soc. Rev.* **2014**, *43*, 5415; b) H. Furukawa, U. Müller, O. M. Yaghi, *Angew. Chem. Int. Ed.* **2015**, *54*, 3417; *Angew. Chem.* **2015**, *127*, 3480; c) Q.-L. Zhu, Q. Xu, *Chem. Soc. Rev.* **2014**, *43*, 5468; d) T. Islamoglu, S. Goswami, Z. Li, A. J. Howarth, O. K. Farha, J. T. Hupp, *Acc. Chem. Res.* **2017**, *50*, 805; e) B. Li, H.-M. Wen, Y. Cui, W. Zhou, G. Qian, B. Chen, *Adv. Mater.* **2016**, *28*, 8819; f) N. Li, J. Liu, J.-J. Liu, L. Dong, Z.-F. Xin, Y.-L. Teng, Y.-Q. Lan, *Angew. Chem. Int. Ed.* **2019**, *58*, 5226; *Angew. Chem.* **2019**, *131*, 5280; g) J.-D. Xiao, D. Li, H.-L. Jiang, *Sci. Sin. Chim.* **2018**, *48*, 1058.

[6] a) P. Valvekens, F. Vermoortele, D. De Vos, *Catal. Sci. Technol.* **2013**, *3*, 1435; b) A. H. Chughtai, N. Ahmad, H. A. Younus, A. Laypkov, F. Verpoort, *Chem. Soc. Rev.* **2015**, *44*, 6804; c) S. Wang, X. Wang, *Small* **2015**, *11*, 3097; d) Y. Li, H. Xu, S. Ouyang, J. Ye, *Phys. Chem. Chem. Phys.* **2016**, *18*, 7563; e) L. Zeng, X. Guo, C. He, C. Duan, *ACS Catal.* **2016**, *6*, 7935; f) M. A. Nasalevich, C. H. Hendon, J. G. Santaclara, K. Svane, B. van der Linden, S. L. Veber, M. V. Fedin, A. J. Houtepen, M. A. van der Veen, F. Kapteijn, A. Walsh, J. Gascon, *Sci. Rep.* **2016**, *6*, 23676; g) L. Jiao, Y. Wang, H.-L. Jiang, Q. Xu, *Adv. Mater.* **2018**, *30*, 1703663; h) C. Wang, B. An, W. Lin, *ACS Catal.* **2019**, *9*, 130; i) A. Dhakshinamoorthy, Z. Li, H. Garcia, *Chem. Soc. Rev.* **2018**, *47*, 8134; j) J.-D. Xiao, H.-L. Jiang, *Acc. Chem. Res.* **2019**, *52*, 356.

[7] a) H. Wu, Y. S. Chua, V. Krungleviciute, M. Tyagi, P. Chen, T. Yildirim, W. Zhou, *J. Am. Chem. Soc.* **2013**, *135*, 10525; b) F. Vermoortele, B. Bueken, G. Le Bars, B. Van de Voorde, M. Vandichel, K. Houthoofd, A. Vimont, M. Daturi, M. Waroquier, V. Van Speybroeck, C. Kirschhock, D. E. De Vos, *J. Am. Chem. Soc.* **2013**, *135*, 11465; c) G. C. Shearer, S. Chavan, J. Ethiraj, J. G. Vitillo, S. Svelle, U. Olsbye, C. Lamberti, S. Bordiga, K. P. Lillerud, *Chem. Mater.* **2014**, *26*, 4068; d) G. C. Shearer, S. Chavan, S. Bordiga, S. Svelle, U. Olsbye, K. P. Lillerud, *Chem. Mater.* **2016**, *28*, 3749; e) M. J. Cliffe, W. Wan, X. Zou, P. A. Chater, A. K. Kleppe, M. G. Tucker, H. Wilhelm, N. P. Funnell, F.-X. Coudert, A. L. Goodwin, *Nat. Commun.* **2014**, *5*, 4176; f) D. S. Sholl, R. P. Lively, *J. Phys. Chem. Lett.* **2015**, *6*, 3437; g) S. Dissegna, K. Epp, W. R. Heinz, G. Kieslich, R. A. Fischer, *Adv. Mater.* **2018**, *30*, 1704501; h) C. A. Trickett, K. J. Gagnon, S. Lee, F. Gándara, H.-B. Bürgi, O. M. Yaghi, *Angew. Chem. Int. Ed.* **2015**, *54*, 11162; *Angew. Chem.* **2015**, *127*, 11314; i) M. R. DeStefano, T. Islamoglu, S. J. Garibay, J. T. Hupp, O. K. Farha, *Chem. Mater.* **2017**, *29*, 1357; j) R. Wei, C. A. Gaggioli, G. Li, T. Islamoglu, Z. Zhang, P. Yu, O. K. Farha, C. J. Cramer, L. Gagliardi, D. Yang, B. C. Gates, *Chem. Mater.* **2019**, *31*, 1655; k) L. Liu, Z. Chen, J. Wang, D. Zhang, Y. Zhu, S. Ling, K.-W. Huang, Y. Belmabkhout, K. Adil, Y. Zhang, B. Slater, M. Eddaoudi, Y. Han, *Nat. Chem.* **2019**, *11*, 622; Y. Han, *Nat. Chem.* **2019**, *11*, 622.

[8] M. Kandiah, M. H. Nilsen, S. Usseglio, S. Jakobsen, U. Olsbye, M. Tilset, C. Larabi, E. A. Quadrelli, F. Bonino, K. P. Lillerud, *Chem. Mater.* **2010**, *22*, 6632.

[9] a) A. De Vos, K. Hendrickx, P. Van Der Voort, V. Van Speybroeck, K. Lejaeghere, *Chem. Mater.* **2017**, *29*, 3006; b) K. L. Svane, J. K. Bristow, J. D. Galeb, A. Walsh, *J. Mater. Chem. A* **2018**, *6*, 8507.

[10] a) Z. Guo, C. Xiao, R. V. Maligal-Ganesh, L. Zhou, T. W. Goh, X. Li, D. Tesfagaber, A. Thiel, W. Huang, *ACS Catal.* **2014**, *4*, 1340; b) J.-D. Xiao, Q. Shang, Y. Xiong, Q. Zhang, Y. Luo, S.-H. Yu, H.-L. Jiang, *Angew. Chem. Int. Ed.* **2016**, *55*, 9389; *Angew. Chem.* **2016**, *128*, 9535.

[11] a) K. Wu, H. Zhu, T. Lian, *Acc. Chem. Res.* **2015**, *48*, 851; b) B. Wu, J. Hu, P. Cui, L. Jiang, Z. Chen, Q. Zhang, C. Wang, Y. Luo, *J. Am. Chem. Soc.* **2015**, *137*, 8769; c) Q. Zhang, Y. Luo, *High Power Laser Sci. Eng.* **2016**, *4*, e22; d) Q. Shang, X. Fang, H.-L. Jiang, Q. Zhang, *Chin. J. Chem. Phys.* **2018**, *31*, 613; e) J. Wang, T. Ding, K. Wu, *J. Am. Chem. Soc.* **2018**, *140*, 7791; f) B. Pattengale, D. J. SantaLucia, S. Yang, W. Hu, C. Liu, X. Zhang, J. F. Berry, J. Huang, *J. Am. Chem. Soc.* **2018**, *140*, 11573.

[12] a) W. Zhou, F. Sun, K. Pan, G. Tian, B. Jiang, Z. Ren, C. Tian, H. Fu, *Adv. Funct. Mater.* **2011**, *21*, 1922; b) Y. Guo, J. Li, Y. Yuan, L. Li, M. Zhang, C. Zhou, Z. Lin, *Angew. Chem. Int. Ed.* **2016**, *55*, 14693; *Angew. Chem.* **2016**, *128*, 14913.

Manuscript received: June 6, 2019
Accepted manuscript online: July 7, 2019
Version of record online: August 1, 2019

